Thermophysics and Aeromechanics, *2016*, *Vol. 23*, *No. 1*

DOI: 10.1134/S0869864316010042

Computation of leading edge film cooling from a CONSOLE geometry (CONverging Slot hOLE)

A. Guelailia, A. Khorsi, and M.K. Hamidou

University of Sciences and Technologies, *Oran*, *Algeria*

E-mail: guelailia@yahoo.fr

(*Received July 21*, *2014*; *in revised form November 5*, *2014*)

The aim of this study is to investigate the effect of mass flow rate on film cooling effectiveness and heat transfer over a gas turbine rotor blade with three staggered rows of shower-head holes which are inclined at 30° to the spanwise direction, and are normal to the streamwise direction on the blade. To improve film cooling effectiveness, the standard cylindrical holes, located on the leading edge region, are replaced with the converging slot holes (console). The ANSYS CFX has been used for this computational simulation. The turbulence is approximated by a k-ε model. Detailed film effectiveness distributions are presented for different mass flow rate. The numerical results are compared with experimental data.

Key words: gas turbine blade, film cooling efficiency, numerical simulation, mass flow rate, cylindrical and converging slot holes.

Introduction

Higher performance of future gas turbines requires an improvement of efficiencies, which are usually achieved by increasing the turbine inlet temperatures. However, the turbine inlet temperatures are generally above the material failure limit of turbine blades (about 1600 K) and thus, demands newer cooling methods that reduce thermal loads on the turbine blades. Methods such as film cooling and internal cooling have led to improvements in modern gas turbine performance. In film cooling, the cooling air bled from the compressor is discharged through holes in the turbine blade wall or the end wall. The injected coolant from holes form a thin thermal insulation layer on the blade surface to protect the blade from being overheated by the hot gas flow from the combustor. A film cooling process depends on many parameters. Primary physical properties, that influence film cooling, are: a coolant-to-hot mainstream velocity ratio, blowing ratio [1], momentum ratio, pressure ratio, temperature ratio, density ratio and turbulence intensity [2,3]. Also, the geometrical characteristics have a bearing on film cooling. Therefore, a geometry of an airfoil and film cooling holes, their distribution and location have been widely studied. In a typical gas turbine airflow, the pressure ratio varies from 1.02 to 1.10, while the corresponding blowing ratio takes values approximately from 0.5 to 2.0. The temperature ratio is within 0.5, 0.85 and the corresponding density ratio varies approximately from 2.0 to 1.5 [4]. There have been numerous experimental and several numerical investigations for the prediction of film cooling effectiveness in literature. These studies are conducted either for flat plate and/or leading edge turbine blades. Among the earlier studies,

© A. Guelailia, A. Khorsi, and M.K. Hamidou, 2016

the authors of the work [5] investigated film cooling of flat plate from one and two rows of simple and compound angle holes. This research has shown that compound angle injection provide better film-cooling protection than the simple angle injection for the same blowing ratio. To our knowledge, investigations on console film cooling were mainly performed on flat plate model and a few investigations have been conducted on film cooled curved surfaces with converging slot-holes. The authors of [6] numerically investigated three different film cooling holes geometries in flat plate. It was found that the console film-cooling geometry presents a very promising improvement in thermal performance. The film-cooling performance of the console rows on a nozzle vane when all the hole rows were open was measured in the work [7]. An experiment was made in [8] for the film cooling of single console row on both suction side and pressure side of blade. However, the information about the influences of some factors on the film cooling performance of consoles on the curved surface was not enough especially in the leading edge region. The authors of the works [9–11] studied the effects of surface roughness on adiabatic effectiveness using a flat plate and saw little degradation in adiabatic effectiveness. The works [12–15] presented the detailed experimental data of the film cooling effectiveness and heat transfer coefficient for single and rows of holes in a flat plate. The heat transfer on the pressure and suction sides as well as on the hub platform surface for a rotating turbine model was studied in [16]. Enhanced heat transfer was observed on the platform due to the secondary flow effects. The film cooling effectiveness on the leading edge of a rotating blade was investigated in the works [17,18]. The cooling performance of a standard cylindrical hole and diffused shaped hole at the stagnation line was investigated numerically in [19, 20]. Seven different film cooling holes at the leading edge of a rotor blade with two rows, one on the pressure side and the other on the suction side were investigated numerically in [21]. It was found that the coolant trace on the suction side was much longer with lower effectiveness than that on the pressure side. An experimental investigation around the film cooled leading edge of a high pressure gas turbine rotor blade has been made in the work [22]. However, several other studies with the same blade have been performed to investigate the influence of many parameters, such as the effect of coolant temperature and mass flow [23], the effect of turbulence models [24], the effect of hole physics [25] and heat exchange peculiarities [26–28].

The focus from this study is to investigate film cooling effectiveness and heat transfer over a VKI gas turbine rotor blade with two different geometries of hole (cylindrical and converging slot hole) at various mass flow rate using a k-ε turbulence model. The predicted results are compared with the experimental results of [22].

Numerical method

The simulations were performed using the CFX software from ANSYS, Inc. In the solver package, the solution of the Reynolds averaged Navier–Stokes equations is obtained by using finite volume method to discretize the continuity, momentum, and energy equations. CFX solves all conservation equations in one linear equation system, with all equations being fully coupled. The calculation is continued until the convergence criterion (10^{-5}) is met.

In this study, the turbulence is modeled by a standard k-ε model. Many researchers use it taking into account its efficiency [29–31]. It has proven optimal for computations and is widely accepted in the practice of computation of gas turbines [32].

It is based on the eddy viscosity concept which assumes that the Reynolds stresses $-\rho\overline{u_i u_j}$ can be expressed in terms of the mean velocity gradients and the eddy or turbulent viscosity μ_t in a manner analogous to the viscous stresses τ_{ij} for laminar Newtonian flows. This model assumes that the eddy viscosity μ_t is linked to the turbulent kinetic energy k and its dissipation rate ε through the following relation:

$$\mu_{\mathrm{t}} = \rho C_{\mu} \frac{k^2}{\varepsilon},$$

where $C_{\mu} = 0.09$, and k and ε are defined, respectively, through the following equations:

$$\frac{\partial(\rho k)}{\partial t} + \frac{\partial(\rho U_j k)}{\partial x_j} = P_k - \rho\varepsilon + \frac{\partial}{\partial x_j}\left(\Gamma_k \frac{\partial k}{\partial x_j}\right),$$

$$\frac{\partial(\rho\varepsilon)}{\partial t} + \frac{\partial(\rho U_j \varepsilon)}{\partial x_j} = \frac{\varepsilon}{k}\left(C_{\varepsilon 1} P_k - C_{\varepsilon 2}\rho\varepsilon\right) + \frac{\partial}{\partial x_j}\left(\Gamma_{\varepsilon} \frac{\partial \varepsilon}{\partial x_j}\right) \text{ with } \Gamma_k = \mu + \mu_{\mathrm{t}}/\sigma_k, \quad \Gamma_{\varepsilon} = \mu + \mu_{\mathrm{t}}/\sigma_{\varepsilon}.$$

In these equations, P_k represents the turbulence production, and $\sigma_{\varepsilon} = 1.3$, $\sigma_k = 1$, $C_{\varepsilon 1} = 1.44$, $C_{\varepsilon 2} = 1.92$ are constants determined experimentally from a wide range of turbulent flows [33].

Geometry

The blade used in the present work is the VKI rotor which has been studied experimentally in the work [22]. The geometry of the blade is illustrated in Fig. 1. The converging slot hole configuration is presented in Fig. 2. The cylindrical and converging slots at the blade leading edge are denoted, respectively, as case 1 and case 2 within the framework of the present numerical simulation (see Fig. 3). For case 1 which corresponds to the baseline configuration, there are three staggered rows of showerhead cooling holes with a diameter d = 0.8 mm. In the spanwise direction, the holes are inclined 30° from the tangential direction. The row and hole spacings were both 2.48 mm and are located at $S/C = -0.031$, 0, 0.031, where S is the length along the blade from the stagnation point and $S/C = 0$ is the blade stagnation line. Similar data were used for the case of converging slots. The exit hole area for case 2 is similar to the first case.

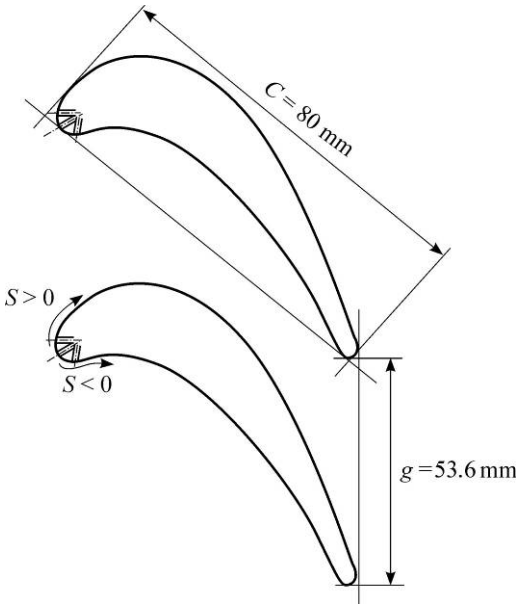

Fig. 1. Geometry of the blade.

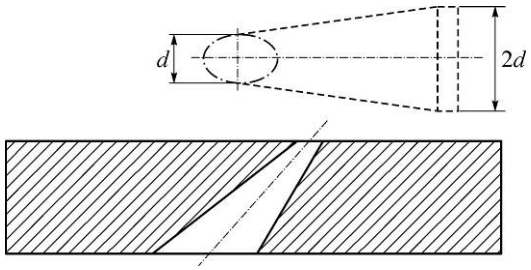

Fig. 2. The converging slot hole configuration.

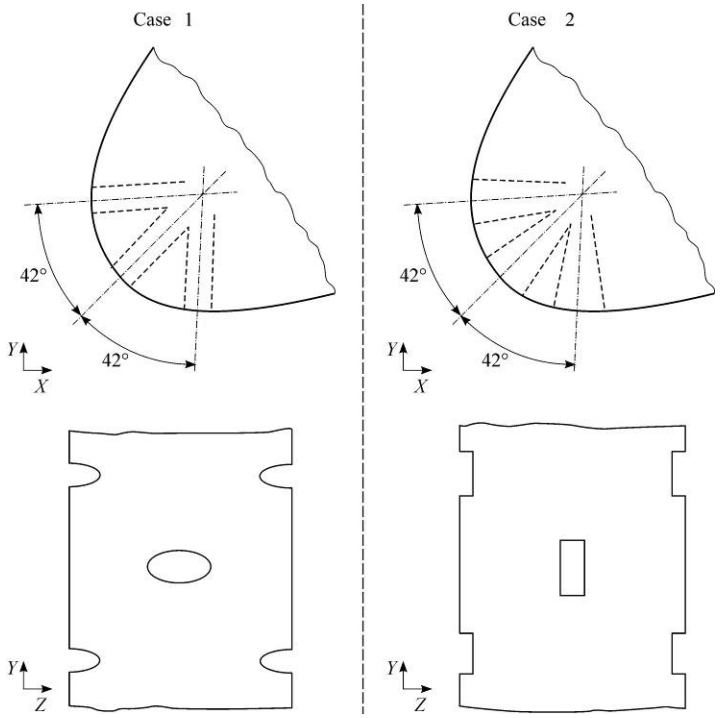

Fig. 3. Leading edge region of the two configurations.

Mesh generation

The computational grid has been obtained using the commercial grid generator ICEM. The numerical domain is discretized using a structured multi-block grid. The final grid adopted for calculations was obtained after a series of tests. It consists of 572 960 and 699 717 grid nodes for cases 1 and 2, respectively. The distribution of the computational nodes was highly refined near the blade. Due to the importance of the region in the vicinity of the hole injection, the computational grid was highly refined in this place. Also, the quality of the computational grid is highly improved by use of the well known O-grid strategy. The normalized y^+ values at the near wall node are kept within $20 < y^+ < 100$. Figure 4 shows the multi-block grid used for this simulation and the zoomed region in the vicinity of the injection hole.

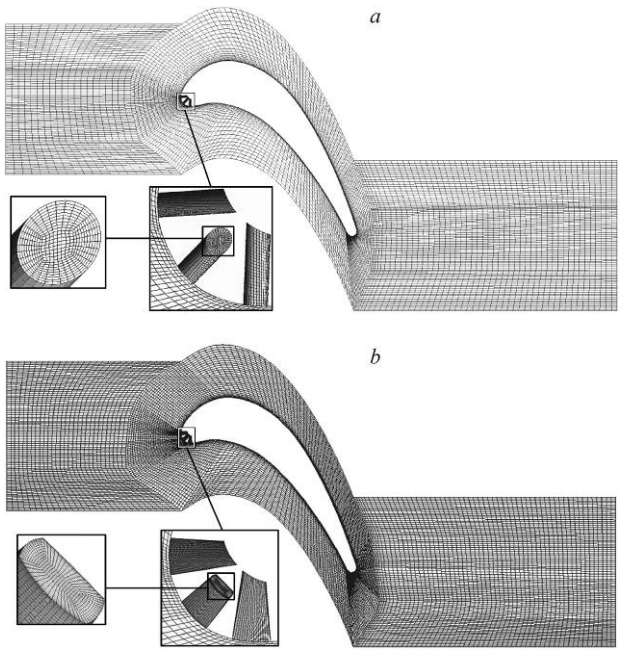

Fig. 4. Computational grid.
a — case 1, *b* — case 2.

Boundary conditions

Details on the boundary conditions and parameters of the blade are given in the Table. Boundary conditions are prescribed at all boundaries of the computational domain. The symmetry conditions are used for the top and bottom planes bounding the domain. At the two periodic boundaries of the turbine cascade, translational periodicity is applied. The flow inlet is defined as the total pressure and the total temperature, while the outlet was defined as a static pressure. The turbulence intensity was set at 5 %. In order to simulate the prevailing conditions in The injection flow boundary region, The velocity is computed according to the mass flow ratio values, while the temperature difference of 48 % between the main stream and the injection flow is considered, such as to match the corresponding experimental conditions. The walls are considered as adiabatic walls with no slip conditions. Air was taken as a working fluid.

Table

Simulation parameter conditions

Boundary conditions		Physical parameters	
P_0, kPa	289.5	d, mm	0.8
T_0, K	409.5	C, mm	80
T_w/T_0	0.727		
T_c/T_0	0.52		
$M = m_c/m_0$, %	1 to 8		

Results and discussion

In the present work, the results of adiabatic and laterally averaged film cooling effectiveness which are defined respectively by equations (1) and (2) were investigated at different mass flow ratios depending on operating conditions as shown in the Table.

$$\eta = (T_0 - T)/(T_0 - T_c), \tag{1}$$

$$\bar{\eta} = \frac{1}{L}\int_L \eta dz, \tag{2}$$

where L represents the spanwise dimension. The simulation was done at different mass flow ratios depending on operating conditions as shown in the Table.

The simulated laterally averaged heat transfer coefficient on the cooled blade surface for the coolant mass flow rate of 0.62% of the main flow rate, and the ratio of coolant temperature to mainstream stagnation temperature of 0.52 is compared with the experimental data of [22] as shown in Fig. 5. The comparison is satisfactory on the pressure side and on the major part of the suction side. Nevertheless,

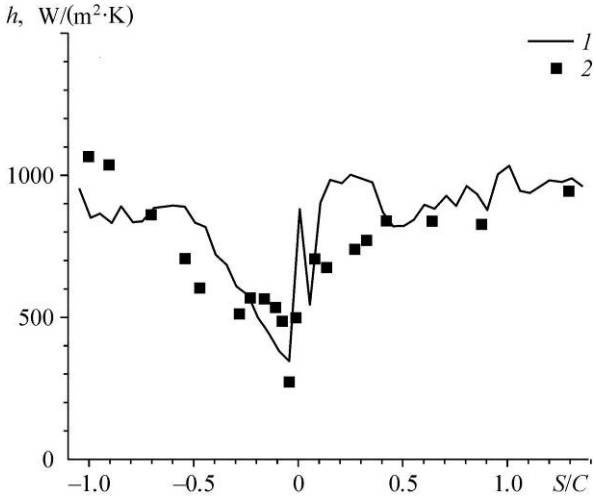

Fig. 5. Laterally averaged heat transfer coefficient (case 1).

1 — present computation, *2* — experimental data of the work [22].

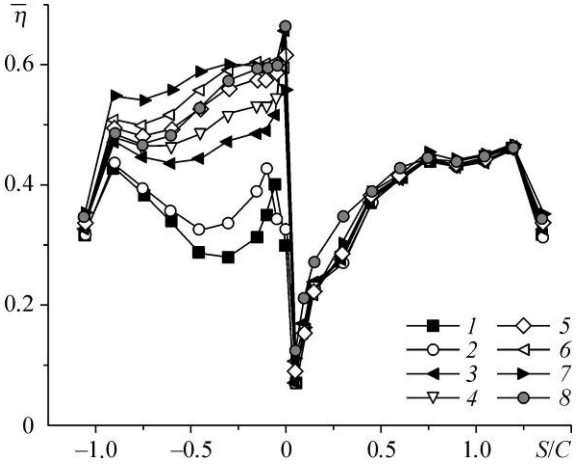

Fig. 6. Laterally averaged effectiveness at various coolant mass flow rates (case 1).
M = 1 (*1*), 2 (*2*), 3 (*3*), 4 (*4*), 5 (*5*), 6 (*6*), 7 (*7*), 8 (*8*).

small differences can be depicted in the front part of the suction side. It can be seen also that the comparison of the predicted heat transfer coefficient in the leading edge region between the rows of holes is not possible due to the lack of experimental data in this narrow region. On the other side, the results from the present study agreed reasonably well with experimental data.

Figure 6 presents the laterally averaged adiabatic film effectiveness at different mass flow ratios for case 1 (cylindrical hole). It can be seen that on the suction side, the film cooling effectiveness is not influenced by the mass flow rate. However, on the pressure side, the film cooling effectiveness is proportional to the mass flow rate until an optimum of 7, after that the tendency is inverted and lower values were found for a mass flow rate of 8.

The area-average film cooling effectiveness obtained from a cylindrical hole (case 1) is shown in Fig. 7. No significant variation of area average effectiveness can be cited on the suction side. On the contrary, the effectiveness on the pressure side is highly affected by mass flow ratio. A maximum value is that given by a mass flow rate of 7.

The laterally averaged adiabatic effectiveness for different mass flow ratios at the leading edge region is shown in Fig 8. It is clear that the film cooling effectiveness of case 2 has a maximum value at M = 8. A decrease of the laterally averaged adiabatic film cooling effectiveness is observed for higher mass flow rate, which is about 9. This reduction is due to the strong penetration of the coolant in the main hot flow when increasing the mass flow rate.

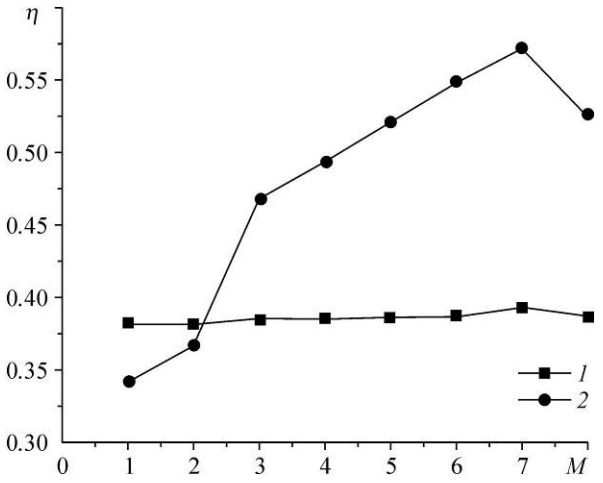

Fig. 7. Area averaged effectiveness at various mass flow rates (case 1).
1 — suction side, *2* — pressure side.

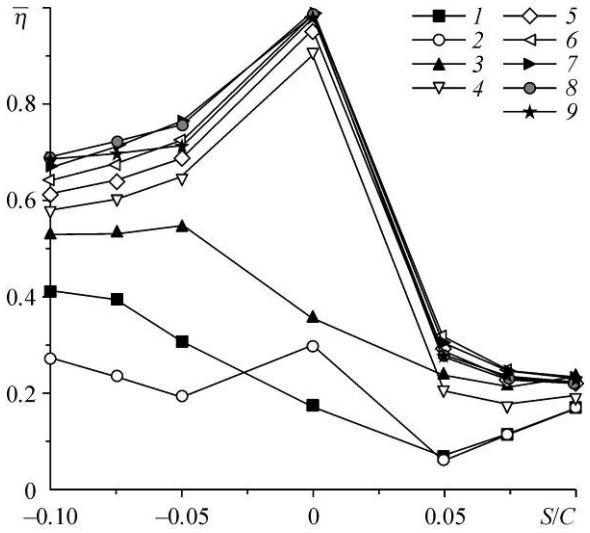

Fig. 8. Laterally averaged cooling effectiveness at various mass flow rates for the blade leading edge region (case 2).
M = 1 (*1*), 2 (*2*), 3 (*3*), 4 (*4*), 5 (*5*), 6 (*6*), 7 (*7*), 8 (*8*), 9 (*9*).

To compare between the two cases, the variation of the laterally averaged film cooling effectiveness is shown at different mass flow ratios in Fig. 9. For all mass flow rates, the average lateral effectiveness provided from case 2 which represents the converging slot hole is better than that obtained from case 1 especially in the near hole region. The zone between the holes is exposed directly to the hot gases hence the lowest values of film cooling effectiveness is located in this region.

Based on the present simulation, Figure 10 shows the lateral film cooling effectiveness distributions for M=7 with a comparison between the two configurations. This distribution is presented at four positions at the leading edge region. Seemingly, for all mass flow rates, the coolant injection from converging slot hole geometry promises a greater lateral film

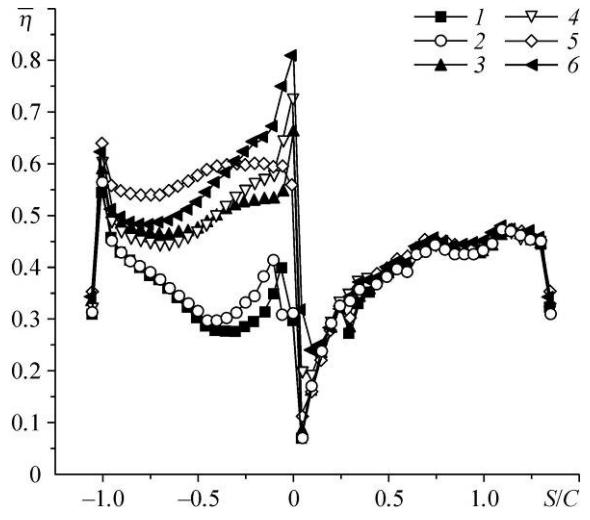

Fig. 9. Laterally averaged cooling effectiveness at various mass flow rates.
Case 1: *M* = 1 (*1*), 4 (*3*), 7 (*5*); case 2: *M* = 1 (*2*), 4 (*4*), 7 (*6*).

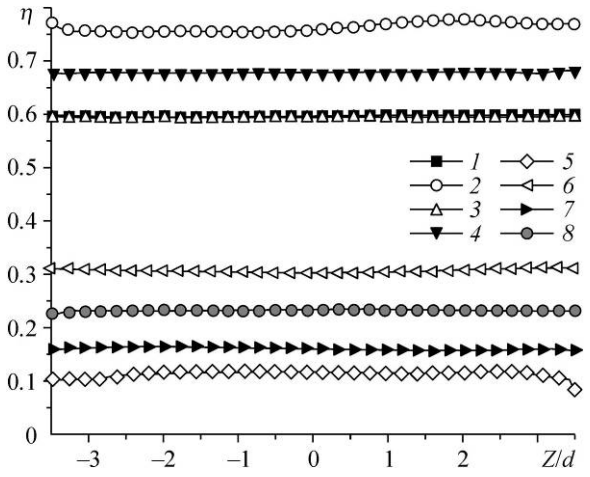

Fig. 10. Film cooling effectiveness at $M = 7$.

Case 1: $S/C = -0.05$ (*1*), -0.1 (*3*), 0.05 (*5*), 0.1 (*7*); case 2: $S/C = -0.05$ (*2*), -0.1 (*4*), 0.05 (*6*), 0.1 (*8*).

cooling effectiveness than the injection from cylindrical hole, this is due to the velocity increase in lateral direction when the coolant is injected from the console. Therefore, the coolant flow is more accelerated and its velocity increases. In the longitudinal direction, the console hole diverges and allows a more uniform distribution of the coolant compared to the cylindrical hole. The difference of film cooling effectiveness between the two cases is more important at the pressure side. The behavior of the effectiveness distribution is typically uniform and takes its highest values at a mass flow ratio of 7.

The contours of film effectiveness distributions for the two cases in the leading edge region at M=7 are shown in Fig 11. The console adiabatic effectiveness shows that the console flow is more uniform than discrete holes. Thus, a better film coverage is obtained by this configuration compared with the cylindrical hole. It is also clear that the cooled area in the vicinity of the console hole is greater than that obtained by the cylindrical hole. The injectant flow trajectory is highly skewed in case 1 especially in the suction side row, this deviation is smaller in case 2. However, the pressure side region is relatively well cooled in comparison with the suction side. This can be attributed to the blade curvature which allows a vortex formation

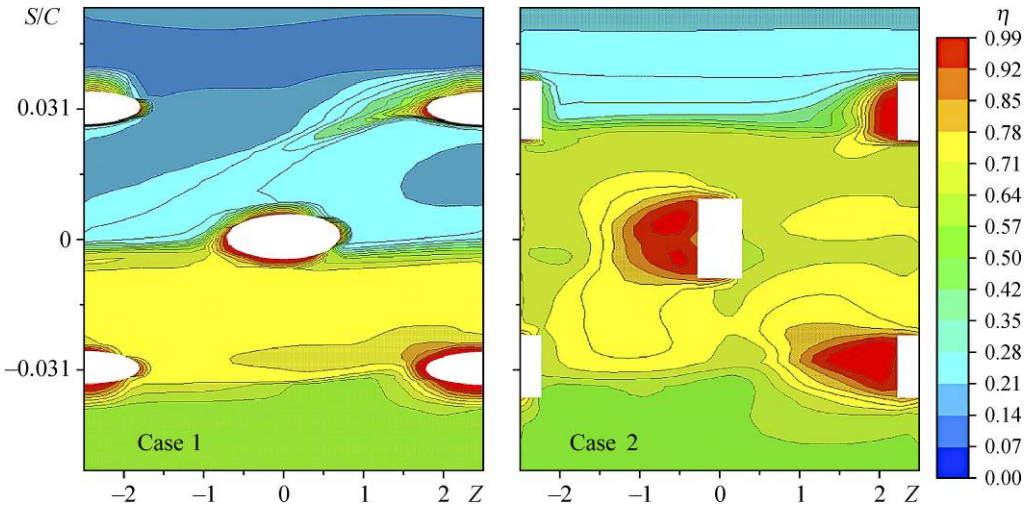

Fig. 11. Film cooling effectiveness distributions in the leading edge region (at $M = 7$).

in this region. The mixture of both main and secondary flows results a lower temperature than the main flow temperature in the vicinity of the pressure side region. Hence, the heat exchange between the blade wall and fluid flow is reduced with the decrease of the temperature difference, that's why the film cooling effectiveness increases.

Conclusion

To improve the film cooling performance by converging slot injection holes for the turbine blade leading edge region, we have studied numerically the film cooling characteristics using cylindrical and converging slot hole body model with three staggered rows. The k-ε turbulence model has been employed to simulate the three dimensional flow field and the film cooling effectiveness by ANSYS CFX code. An acceptable agreement with previous experimental measurements has been obtained in terms of heat transfer coefficient. The film cooling effectiveness from a cylindrical hole (case 1), and converging slot hole (case 2) was presented with a comparison between the two cases for different mass flow rates. It is noted that the mass flow rate has a very strong effect on film cooling effectiveness, and injectant trajectory is sensitive to it. For a typical cylindrical hole, it is observed that the injectant lifts off and separates from the surface as the mass flow rate increases. The film cooling performance can be significantly improved by controlling the injection hole shape. The console (case 2) shows much higher film cooling effectiveness because of strong lateral momentum of the injectant by spanwise diffusion of the hole exit. Under the same condition and for the two cases, the cooling effectiveness on the pressure side is more important than the suction side. As well, the mass flow rate has no significant effect on the film cooling effectiveness in the suction side, in contrast of the suction side, increasing mass flow rate provokes an increase of film cooling effectiveness in the pressure side.

Nomenclature

C — chord length,
d — coolant hole diameter,
h — heat transfer coefficient based on $(T_0 - T_w)$,
k — turbulence kinetic energy,
M — mass flow rate,
P — pressure,
S — distance from the leading edge along the pressure or suction surface,
T — temperature,
ε — rate of kinetic energy dissipation,
η — film-cooling effectiveness,
ρ — density.

Subscripts and superscripts

0 — free stream conditions,
c — injection conditions,
$\bar{}$ — averaged value,
w — value at wall.

References

1. **U. Drost and A. Bölcs,** Investigation of detailed film cooling effectiveness and heat transfer distributions on a gas turbine airfoil, ASME J. Turbomachinery, 1999, Vol. 121, P. 233–242.
2. **H.D. Ammari, N. Hay, and D. Lampard,** The effect of density ratio on the heat transfer coefficient from a film-cooled flat plate, ASME J. Turbomachinery, 1990, Vol. 112, P. 444–450.
3. **A.K. Sinha, D.G. Bogard, and M.E. Crawford,** Film-cooling effectiveness downstream of a single row of holes with variable density ratio, ASME J. Turbomachinery, 1991, Vol. 113, P. 442–449.
4. **J.C. Han, S. Dutta, and S.V. Ekkad,** Gas turbine heat transfer and cooling technology, Taylor & Francis, London, 2000.
5. **A. Azzi, M. Abidat, and B.A. Jubran,** Film cooling predictions of simple and compound angle injection from one and two staggered rows, Numerical Heat Transfer. Part A: Applications, 2001, Vol. 40, No. 3, P. 273–294.
6. **A. Khorsi and A. Azzi,** Computation film cooling from three different holes geometries, MECHANIKA, 2010, No. 6, P. 32–37.
7. **J.E. Sargison, S.M. Guo, M.L.G. Oldfield, G.D. Lock, A.Y. Rawlinson, and D.Ch. Xu,** A converging slot-hole film-cooling geometry. Part 2. Transonic nozzle guide vane heat transfer and loss, ASME J. Turbomachinery, 2002, Vol. 124, P. 461–471.

8. **C.L. Liu, H.R. Zhu, J.T. Bai, and D.Ch. Xu,** Film cooling performance of converging slot-hole rows on a gas turbine blade, Int. J. Heat Mass. Transf., 2010, Vol. 53, P. 5232–5241.
9. **R.J. Goldstein, E.R.G. Eckert, H.D. Chiang, and E. Elovic,** Effect of surface roughness on film cooling performance, ASME J. Engng Gas Turbines Power, 1985, Vol. 107, P. 111–116.
10. **D.L. Schmidt and D.G. Bogard,** Effects of free-stream turbulence and surface roughness on film cooling, ASME Paper, 1996, No. 96-GT–462.
11. **D.L. Schmidt, B. Sen, and D.G. Bogard,** Effects of surface roughness on film cooling, ASME Paper, 1996, No. 96-GT-299.
12. **C.H.N. Yuen and R.F. Martinez-Botas,** Film cooling characteristics of a single round hole at various streamwise angles in a crossflow. Part I. Effectiveness, Int. J. Heat Mass Transfer, 2003, Vol. 46, P. 221–235.
13. **C.H.N. Yuen and R.F. Martinez-Botas,** Film cooling characteristics of a single round hole at various streamwise angles in a crossflow. Part II. Heat transfer coefficients, Int. J. Heat Mass Transfer, 2003, Vol. 46, P. 237–249.
14. **C.H.N. Yuen and R.F. Martinez-Botas,** Film cooling characteristics of rows of round holes at various streamwise angles in a crossflow. Part I. Effectiveness, Int. J. Heat Mass Transfer, 2005, Vol. 48, P. 4995–5016.
15. **C.H.N. Yuen and R.F. Martinez-Botas,** Film cooling characteristics of rows of round holes at various streamwise angles in a crossflow. Part II. Heat transfer coefficients, Int. J. Heat Mass Transfer, 2005, Vol. 48, P. 5017–5035.
16. **M.F. Blair,** An experimental study of heat transfer in a large-scale turbine rotor passage, ASME J. Turbomachinery, 1994, Vol. 116, P. 1–13.
17. **J. Ahn, M.T. Schobeiri, J.C. Han, and H.K. Moon,** Film cooling effectiveness on the leading edge of a rotating turbine blade, ASME Paper No. IMECE. 2004-59852, 2004.
18. **J. Ahn, M.T. Schobeiri, J.C. Han, and H.K. Moon,** Film cooling effectiveness on the leading edge of a rotating film-cooled blade using pressure sensitive paint, ASME Paper No. GT-2005-68344, 2005.
19. **W.D. York and J.H. Leylek,** Leading-edge film-cooling physics. Part I. Adiabatic effectiveness, ASME Paper No. 2002-GT-30166, 2002.
20. **W.D. York and J.H. Leylek,** Leading-edge film-cooling physics. Part II. Heat transfer coefficient, ASME Paper No. 2002-GT-30167, 2002.
21. **S.B. Islami, A. Tabrizi, B. Jubran, and E. Esmaeilzadeh,** Influence of trenched shaped holes on turbine blade leading edge film cooling, Heat Transfer Engng, 2010, Vol. 31, No. 10, P. 889–906.
22. **C. Camci and T. Arts,** Experimental heat transfer investigation around the film-cooled leading edge of a high-pressure gas turbine rotor blades, J. Engng Gas Turbine Power, 1985, Vol. 107, P. 1016–1021.
23. **V.K. Garg,** Effect of coolant temperature and mass flow on film cooling of turbine blades, Int. J. Heat and Fluid Flow, 1997, Vol. 40, No. 2, P. 435–445.
24. **V.K. Garg,** Heat transfer on a film cooled rotating blade using different turbulence models, Int. J. Heat and Fluid Flow, 1999. Vol. 42, P. 789–802.
25. **V.K. Garg,** Heat transfer on a film-cooled blade effect of hole physics, Int. J. Heat and Fluid Flow, 1999, Vol. 20, P. 10–25.
26. **V.K. Garg,** Comparison of predicted and experimental Nusselt number for a film cooled rotating blade, Int. J. Heat and Fluid Flow, 1997, Vol. 18, P. 452–460.
27. **V.K. Garg,** Heat transfer on a film-cooled rotating blade, Int. J. Heat and Fluid Flow, 2000, Vol. 21, P. 134–145.
28. **V.K. Garg,** Modeling film-coolant flow characteristics at the exit of shower-head holes, Int. J. Heat and Fluid Flow, 2001, Vol. 22, P. 134–142.
29. **Y. Chengfenga and Z. Jingzhoub,** Influence of multi-hole arrangement on cooling film development, Chinese J. Aeronautics, 2012, Vol. 25, P. 182–188.
30. **R. Hasan and A. Puthukkudi,** Numerical study of effusion cooling on an adiabatic flat plate, Propulsion and Power Research, 2013, Vol. 2, No. 4, P. 269–275.
31. **I. Koc, C. Parmaksızoglu, and M. Cakan,** Numerical investigation of film cooling effectiveness on the curved surface, Energy Conversion and Management, 2006, Vol. 47, P. 1231–1246.
32. **M. Silieti, E. Divo, and A.J. Kassab,** The effect of conjugate heat transfer on film cooling effectiveness, Numerical Heat Transfer. Part B, 2009, Vol. 56, P. 335–350.
33. **S.V. Patankar and D.B. Spalding,** A calculation procedure for heat, mass and momentum transfer in three-dimensional parabolic flows, Int. J. Heat and Mass Transfer, 1972, Vol. 15, P. 1778–1806.